Title	Analysis and Design of Highly Efficient Wideband RF-Input Sequential Load Modulated Balanced Power Amplifier
Authors(s)	Pang, Jingzhou; Li, Yue; Li, Meng; Zhang, Yikang; Zhou, Xin Yu; Dai, Zhijiang; Zhu, Anding
Publication date	2020-05
Publication information	IEEE Transactions on Microwave Theory and Techniques, 68 (5): 1741-1753
Publisher	IEEE
Item record/more information	http://hdl.handle.net/10197/11748
Publisher's statement	© 2020 IEEE. Personal use of this material is permitted. Permission from IEEE must be obtained for all other uses, in any current or future media, including reprinting/republishing this material for advertising or promotional purposes, creating new collective works, for resale or redistribution to servers or lists, or reuse of any copyrighted component of this work in other works.
Publisher's version (DOI)	10.1109/tmtt.2019.2963868

Analysis and Design of Highly-Efficient Wideband RF-Input Sequential Load Modulated Balanced Power Amplifier

Jingzhou Pang, *Member, IEEE,* Yue Li, *Student Member, IEEE,* Meng Li, *Student Member, IEEE,* Yikang Zhang, Xin Yu Zhou, *Member, IEEE,* Zhijiang Dai, *Member, IEEE,* and Anding Zhu, *Senior Member, IEEE*

***Abstract*—The analysis and design of an RF-input sequential load modulated balanced power amplifier (SLMBA) are presented in this paper. Unlike the existing LMBAs, in this new configuration, an over-driven class-B amplifier is used as the carrier amplifier while the balanced PA pair is biased in class-C mode to serve as the peaking amplifier. It is illustrated that the sequential operation greatly extends the high efficiency power range and enables the proposed SLMBA to achieve high back-off efficiency across a wide bandwidth. An RF-input SLMBA at 3.05-3.55 GHz band using commercial GaN transistors is designed and implemented to validate the proposed architecture. The fabricated SLMBA attains a measured 9.5-10.3 dB gain and 42.3-43.7 dBm saturated power. Drain efficiency of 50.9-64.9/46.8-60.7/43.2-51.4% is achieved at 6/8/10 dB output power back-off within the designed bandwidth. By changing the bias condition of the carrier device, higher than 49.1% drain efficiency can be obtained within 12.8 dB output power range at 3.3 GHz. When driven by a 40 MHz OFDM signal with 8 dB peak to average power ratio (PAPR), the proposed SLMBA achieves adjacent channel leakage ratio (ACLR) better than -25 dBc with an average efficiency of 63.2% without digital predistortion (DPD). When excited by a 10-carrier 200 MHz OFDM signal with 10 dB PAPR, the average efficiency can reach 48.2% and -43.9 dBc ACLR can be obtained after DPD.**

***Index Terms*—Load modulated balanced power amplifier, high efficiency, sequential power amplifier, wideband, 5G**

I. Introduction

To improve spectrum efficiency, modulated signals with high peak to average power ratio (PAPR) are usually used in modern wireless communication systems. This creates a strong demand for radio frequency (RF) power amplifiers (PAs) to have high efficiency at output power back-off (OBO). Many PA architectures have been proposed to meet this requirement, such as Doherty power amplifier (DPA), envelope tracking (ET) and out-phasing. Among them, DPA has become one of the most widely used PA architectures in wireless cellular base stations because of its low complexity and high reliability. To support multi-band/multi-mode operation and to accommodate wide signal bandwidth requirement, several bandwidth extension techniques for DPAs have been introduced, such as continuous mode technique [1]–[3], impedance compensation [4], [5], complex combining loads [6] and post-matching structure [7]–[9]. Most wideband DPAs reported to date focus on the symmetric structure [1]–[4], [6]–[12], limiting the efficiency performance at deep back-off region. In forthcoming 5G systems, the output power of the transmitters may need to be dynamically adjusted according to the data traffic and the PAPR of the transmit signals may become higher. It is thus desirable for transmitters to provide high efficiency performance at deep OBO. Moreover, in some new applications, such as small base-stations mounted on unmanned aerial vehicles (UAVs), it is more important to extend the power range with high efficiency performance, because the output power levels of these base-stations are required to be reconfigured based on the specific locations [13].

Recently, a new PA architecture called load modulated balanced amplifier (LMBA) was proposed [14]–[19], where a control signal is injected to a balanced amplifier via a commonly terminated port of the output coupler. The LMBA is able to modulate the impedance seen by the balanced amplifier by varying the amplitude and phase of the external control signal. This enables the power and efficiency of the PA to be optimized dynamically at specific OBO levels. By using wideband couplers as the load modulation networks, the LMBA can potentially achieve high efficiency at different power back-off across a wide bandwidth. This configuration however has certain limitations. For instance, in the reported LMBA architectures, especially the RF-input ones, the balanced power amplifier pair is used as the carrier amplifier. In this case, the efficiency of the PA at OBO may be limited by parallel losses [20]. More importantly, for the balanced carrier PA pair, load conditions at both back-off and saturation should be satisfied. Due to the parasitic and package parameters of transistors, designing output matching networks (OMNs) to satisfy such conditions across a wide bandwidth is often difficult, which can limit the bandwidth of the LMBA to some extent.

In this paper, we propose a new configuration for the RF-

This work was supported in part by the Science Foundation Ireland under Grant Numbers 13/RC/2077, 17/NSFC/4850 and 16/IA/4449. This research was also funded in part by funding from the European Union's Horizon 2020 Research and Innovation Program under the Marie Sklodowska-Curie grant agreement number 713567. (*Corresponding author: Jingzhou Pang*)

J. Pang, Y. Li, M. Li, and A. Zhu are with the School of Electrical and Electronic Engineering, University College Dublin, Dublin 4, Ireland.(e-mail: jingzhou.pang@ucd.ie; yue.li1@ucdconnect.ie; meng.li@ucdconnect.ie; anding.zhu@ucd.ie)

Y. Zhang is with the Department of Electronic and Information Science, University of Science and Technology of China, and also with the Key Laboratory of Electromagnetic Space Information, Chinese Academy of Sciences, Hefei, Anhui, China (e-mail: zyikang@mail.ustc.edu.cn)

X. Y. Zhou is with the Department of Electronic Engineering, City University of Hong Kong, Hong Kong SAR (e-mail: zhouxinyu24@hotmail.com)

Z. Dai is with the School of Microelectronics and Communication Engineering, Chongqing University, Chongqing, China. (e-mail: daizj_ok@126.com)

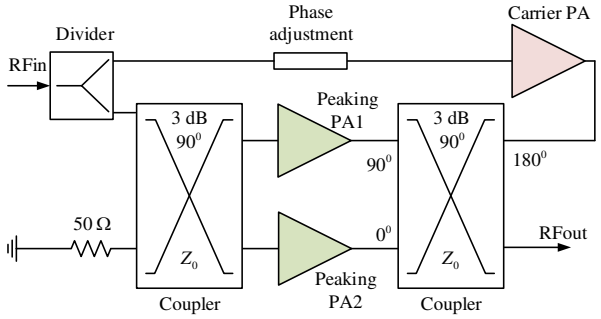

Fig. 1. Block diagram of the proposed SLMBA.

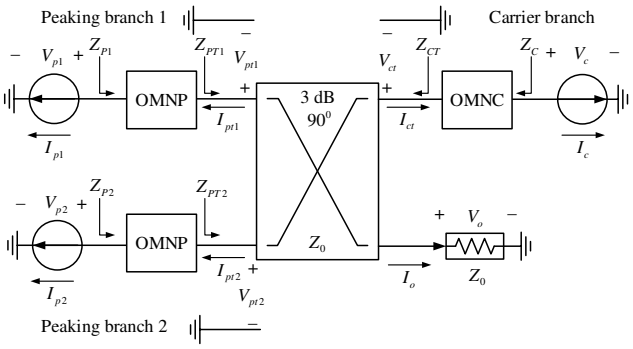

Fig. 2. Theoretical block diagram of the proposed SLMBA.

input LMBA, shown in Fig. 1. In this configuration, a class-B amplifier is used as the carrier amplifier while the balanced PA pair is used as the peaking amplifiers in class-C mode. The carrier amplifier is connected to the isolated port of a 90° directional coupler while the peaking amplifiers are connected to the through and coupled ports, respectively. The two peaking amplifiers form a balanced PA when their output signals have a phase difference of 90°. At the low power region, namely, when the output power is lower than the OBO level, the peaking amplifiers are turned off and the output power of the PA system is provided only by the carrier PA. When the output power is higher than the OBO level, the two peaking PAs are turned on and the carrier PA is to be saturated. When the output power is further increased, additional power increase is mainly provided by the peaking PA pair due to the saturation status of the carrier PA. This leads that the operation of the proposed PA is close to that of the sequential power amplifier (SPA) and thus we name it as Sequential LMBA (SLMBA) here [21]–[23]. In [24], similar bias conditions have been employed to realise a Doherty-like LMBA. However, its operation relies on a reconfigurable phase shifting circuit with additional input at the control path, which makes the system architecture more complex and the dual-input control or the dynamic phase tuning is difficult to implement in a real system. Meanwhile, the efficiency performance was reported at a single operation frequency only and no detailed design procedure was given.

As mentioned earlier, the bandwidth of the conventional LMBA may be limited due to the design difficulties of OMNs. In the proposed SLMBA, load modulation process only occurs in the peaking amplifier branch when the output power reaches the OBO level. This means that for both the carrier and the peaking PAs, the OMNs only need to consider one load condition, which makes the design of broadband matching networks much easier. Moreover, because more power can be generated in the balanced PA than that in the carrier branch, with flexible configurations, the SLMBA can achieve high efficiency at a large power range. The proposed SLMBA therefore has the potential to achieve high back-off efficiency in a large power range across a wide bandwidth.

Compared with other PA architectures that can achieve a large high-efficiency range, such as asymmetrical or multi-stage Doherty PAs [5], [25], the design of the proposed SLMBA is easier due to the constant load condition at the carrier branch. A similar operation of using over-driven carrier amplifiers to design wideband PAs with high back-off efficiency was recently reported in distributed efficiency power amplifiers (DEPAs) [26]–[28] by employing multiple distributed peaking amplifiers and multi-section combiners. In comparison, the proposed SLMBA can realize the similar load and efficiency condition but with a smaller number of peaking devices. A wideband RF-input SLMBA with 3.05-3.55 GHz bandwidth has been designed and implemented. The fabricated PA presents excellent efficiency performance at 10 dB OBO within the design bandwidth. When changing the bias condition of the implemented SLMBA, more than 13 dB high efficiency power range can be achieved.

The remaining part of the paper is organized as follows, Section II presents the operation theory of the proposed RF-input SLMBA. Section III shows the detailed procedures of realizing the SLMBA with commercial GaN transistors on a 31 mil Rogers 5880 substrate. In Section IV, the experimental results are presented with a conclusion given in Section V.

II. Theoretical Analysis of RF-Input SLMBA

To analyze the load modulation process of the proposed SLMBA, the theoretical block diagram of the PA is employed as shown in Fig. 2, where the active devices are represented by using current generators (CGs) and i_{ca} and i_{pk} represents the carrier and peaking current, respectively.

A. Current Generator Model

Because the carrier device is over-driven when the output power is higher than the OBO level, linear current generator (CG) model is not suitable for the proposed architecture. Therefore, a nonlinear model of the CGs must be derived firstly. To simplify the analysis, only magnitudes of the related currents are considered while the phase information are omitted. The phase shifts between different nodes will be added when analyzing the load modulation process.

The carrier current i_{ca} can be defined as,

$$i_{ca}(\beta) = \begin{cases} i_{ca,bo}(\beta) & ,0 \le \beta < \beta_{bo} \\ i_{ca,h}(\beta) & ,\beta_{bo} \le \beta \le 1 \end{cases} \tag{1}$$

where $i_{ca,bo}$ is the carrier drain current when the peaking device is off, and $i_{ca,h}$ is the carrier drain current when the

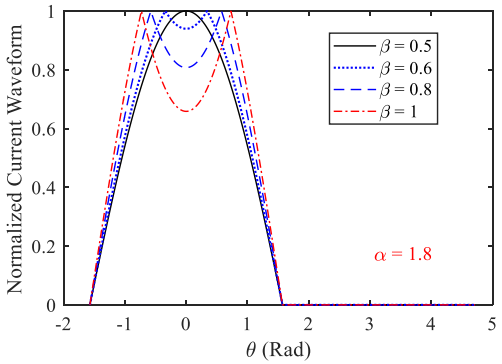

Fig. 3. Normalized carrier current waveform versus different values of β when $\beta_{bo} = 0.5$, $\alpha = 1.8$.

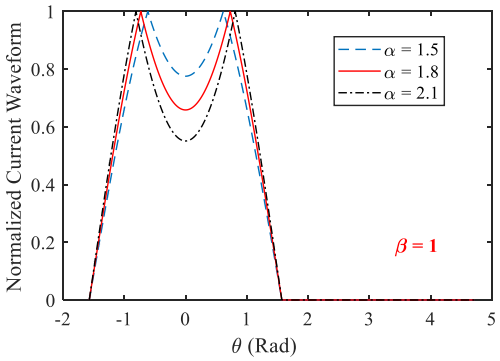

Fig. 4. Normalized carrier current waveform versus different values of α when $\beta_{bo} = 0.5$, $\beta = 1$.

peaking device is on. β is the normalized variable to describe the magnitude of the output current, and β_{bo} is the threshold between the low and high power region. $i_{ca,bo}$ can be simply expressed from the definition of the class-B mode current as,

$$i_{ca,bo}(\beta) = \begin{cases} (\beta/\beta_{bo}) I_{max,c} \cdot \cos\theta & , -\dfrac{\pi}{2} \le \theta < \dfrac{\pi}{2} \\ 0 & , \text{otherwise} \end{cases} \tag{2}$$

The DC and fundamental components of $i_{ca,bo}$ can be obtained by using the Fourier transform as,

$$i_{ca,bo}[0] = \frac{\beta}{\pi\beta_{bo}} I_{max,c} \tag{3}$$

$$i_{ca,bo}[1] = \frac{\beta}{2\beta_{bo}} I_{max,c} \tag{4}$$

Based on the configuration of the proposed PA, the carrier current achieves the maximum linear value $I_{max,c}$ at β_{bo}, and the peaking devices turn on at the same time. When $\beta > \beta_{bo}$, the carrier CG will be over-driven. Therefore, $i_{ca,h}$ can be expressed by using the over-driven current waveform formula as follows,

$$i_{ca,h}(\beta) = \begin{cases} \alpha^{\beta-\beta_{bo}} I_{max,c} \cdot \cos\theta & , -\dfrac{\pi}{2} \le \theta < -\theta_{od} \\ I_{max,c} \cdot (2 - \alpha^{\beta-\beta_{bo}} \cdot \cos\theta) & , -\theta_{od} \le \theta < \theta_{od} \\ \alpha^{\beta-\beta_{bo}} I_{max,c} \cdot \cos\theta & , \theta_{od} \le \theta \le \dfrac{\pi}{2} \\ 0 & , \text{otherwise} \end{cases} \tag{5}$$

where (-θ_{od}, θ_{od}) defines the over-driven phase range and θ_{od} can be calculated as,

$$\theta_{od} = \arccos\left(\alpha^{\beta_{bo}-\beta}\right) \tag{6}$$

where α is the over-driven coefficient, which indicates different over-driven current behaviors.

The above over-driven current formula is a generalized form of the current waveform equation introduced in [29], [30]. As an example, Fig. 3 shows the normalized carrier current waveform versus different values of β when $\beta_{bo} = 0.5$ and $\alpha = 1.8$, demonstrating how the over-driven current changes with β. Only the waveforms at saturation, namely when $\beta_{bo} \ge 0.5$, are given here, since the waveform is just a half sine wave

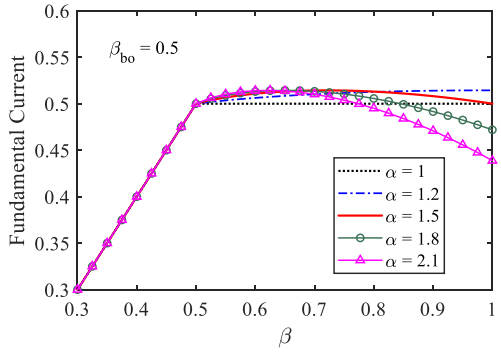

Fig. 5. Fundamental component of the carrier current versus β with different values of α when $\beta_{bo} = 0.5$, $I_{max,c} = 1$.

when $\beta_{bo} < 0.5$. From Fig. 3, we can see that an increasingly severe clipping effect occurs in the waveform with the increase of β.

By using the Fourier transform, the DC and fundamental components of the over-driven current can be obtained as,

$$i_{ca,h}[0] = I_{max,c} \frac{\alpha^{\beta-\beta_{bo}}(1 - 2\sin\theta_{od}) + 2\theta_{od}}{\pi} \tag{7}$$

$$i_{ca,h}[1] = I_{max,c} \frac{8\sin\theta_{od} - \alpha^{\beta-\beta_{bo}}(2\sin 2\theta_{od} + 4\theta_{od} - \pi)}{2\pi}. \tag{8}$$

The over-driven current behavior will change as α changes. Fig. 4 presents the normalized carrier current waveform versus different values of α when $\beta_{bo} = 0.5$ and $\beta = 1$. It can be seen that, the saturated current waveform also presents an increasingly severe clipping effect with the increase of α. To further discuss how the value of α affects the current behavior, the fundamental component of the carrier current versus β with different values of α is presented in Fig. 5, where we can see that, with different values of α, the fundamental component changes as well. Particularly, when $\alpha = 1$, the carrier CG model degenerates into the piecewise linear model used in [26]. Because the fundamental component value of the carrier current affects the required peaking impedance at saturation, it is important to know how to choose the specific value of α. A simple way is to choose α based on the ratio between the value of $i_{ca,h}[1]$ when $\beta = 1$ and $\beta = \beta_{bo}$, i.e., $I_{max,c}/2$. For

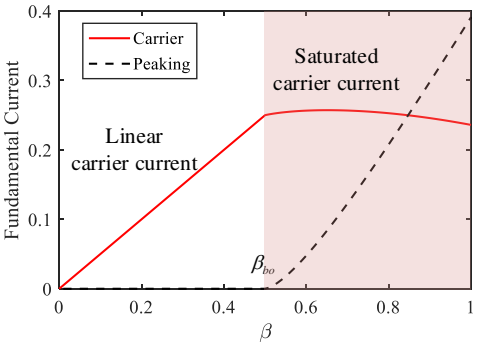

Fig. 6. Fundamental components of i_{ca} and i_{pk} when $\beta_{bo} = 0.5$, $\alpha = 1.8$, $I_{max,c} = 0.5$ and $I_{max,p} = 1$.

example, based on the behavior shown in Fig. 5, if the value of $i_{ca,h}[1]$ at the peak output power of the SLMBA is equal or close to the value at back-off, then $\alpha = 1.5$ can be chosen when $\beta_{bo} = 0.5$.

The two peaking amplifiers are biased at class-C mode, thus i_{pk} can be expressed as,

$$i_{pk}(\beta) = \begin{cases} I_{max,p}\dfrac{\beta\cos\theta - \beta_{bo}}{1-\beta_{bo}}, & -\theta_p \le \theta < \theta_p \\ 0, & \text{otherwise} \end{cases} \tag{9}$$

where (-θ_p, θ_p) defines the turn-on phase range of the peaking devices and θ_p can be calculated as,

$$\theta_p = \arccos\left(\beta_{bo}/\beta\right) \tag{10}$$

Similarly, the DC and fundamental components of the peaking current can be obtained from the Fourier transform as,

$$i_{pk}[0] = \frac{I_{max,p}}{1-\beta_{bo}} \cdot \frac{2\beta\sin\theta_p - 2\beta_{bo}\theta_p}{\pi} \tag{11}$$

$$i_{pk}[1] = \frac{I_{max,p}}{1-\beta_{bo}} \cdot \frac{\beta(2\theta_p + \sin 2\theta_p) - 4\beta_{bo}\sin\theta_p}{2\pi} \tag{12}$$

From (1), (4), (8) and (12), the relationship between the fundamental currents of the carrier and peaking CGs can be clearly described. For the carrier current, it linearly increases to the linear maximum value when $\beta \le \beta_{bo}$ while keeping over-driven when $\beta > \beta_{bo}$. On the other hand, the peaking PA pair is turned on when $\beta > \beta_{bo}$. The above analysis shows that the carrier PA does not generate more power when $\beta > \beta_{bo}$ and thus the increased output power only comes from the peaking PA pair at saturation. This behavior is similar to the sequential PA. To illustrate this operation, Fig. 6 gives the fundamental components of i_{ca} and i_{pk} when $\beta_{bo} = 0.5$, $\alpha = 1.8$, $I_{max,c} = 0.5$ and $I_{max,p} = 1$, as an example.

B. Load Modulation Analysis

After building the model of the related CGs, the load modulation process of the proposed SLMBA can be analyzed. For the coupler, i.e., a lossless four-port network shown in Fig. 2, the voltage and current relationship can be expressed as,

$$\begin{bmatrix} v_o \\ v_{pt1} \\ v_{ct} \\ v_{pt2} \end{bmatrix} = \hat{\mathbf{Z}}_{\mathbf{coupler}} \begin{bmatrix} i_o \\ i_{pt1} \\ i_{ct} \\ i_{pt2} \end{bmatrix} \tag{13}$$

where $\hat{\mathbf{Z}}_{\mathbf{coupler}}$ is the Z-parameter matrix of the 3-dB coupler, which can be expressed as,

$$\hat{\mathbf{Z}}_{\mathbf{coupler}} = Z_0 \begin{bmatrix} 0 & 0 & j & -j\sqrt{2} \\ 0 & 0 & -j\sqrt{2} & j \\ j & -j\sqrt{2} & 0 & 0 \\ -j\sqrt{2} & j & 0 & 0 \end{bmatrix} \tag{14}$$

where Z_0 is the port impedance of the coupler when the matching condition is satisfied.

Let's assume all the employed matching networks are lossless in the matching band. Based on the conservation of energy we can obtain,

$$\begin{cases} i_{pt}/i_p = \sqrt{Z_P/Z_{PT}} \\ v_{pt}/v_p = \sqrt{Z_{PT}/Z_P} \end{cases} \tag{15}$$

$$\begin{cases} i_{ct}/i_c = \sqrt{Z_C/Z_{CT}} \\ v_{ct}/v_c = \sqrt{Z_{CT}/Z_C}. \end{cases} \tag{16}$$

To simplify the analysis, we can define the impedance ratio generated by the carrier and peaking OMNs as $\gamma_c = \sqrt{Z_{CT}/Z_C}$ and $\gamma_p = \sqrt{Z_{PT}/Z_P}$. Because of the required phase difference between the two branches in the balanced PA pair, the current relationship between the two peaking PAs can be expressed as $i_{p1} = i_{pk}$ and $i_{p2} = -j \cdot i_{pk}$. Moreover, in order to keep the pure resistance for the peaking impedance, it is important to set $i_c = j \cdot i_{ca}$.

Based on the above setting, the port impedance can be calculated from (13), (14), (15) and (16) as,

$$Z_{CT} = Z_0 \tag{17}$$

$$Z_{PT1} = Z_{PT2} = Z_0(1 + \sqrt{2}\frac{i_{ca}\gamma_p}{i_{pk}\gamma_c}). \tag{18}$$

The carrier and peaking matching impedance can then be obtained as,

$$Z_C = Z_0/\gamma_c^2 \tag{19}$$

$$Z_{P1} = Z_{P2} = \frac{Z_0}{\gamma_p^2}(1 + \sqrt{2}\frac{i_{ca}\gamma_p}{i_{pk}\gamma_c}). \tag{20}$$

Because Z_0 and γ_c are constant, it is obvious that Z_C is also constant. Therefore, as mentioned early, there is no load modulation for the carrier CG. in the meantime, for the peaking CG, the related impedance gradually decreases from infinity with the increase of i_{pk}. At the low power region, the peaking CG is off, which means $i_{pk} = 0$. From (20) we can know that, Z_P equals to infinity. Therefore, the efficiency of the proposed SLMBA at the low power region is determined only by the carrier PA. At the high power region, i_{ca} no longer grows while i_{pk} gradually increases, which means Z_P will become smaller while Z_C remains the same value from (19). In this situation, the efficiency of the proposed SLMBA

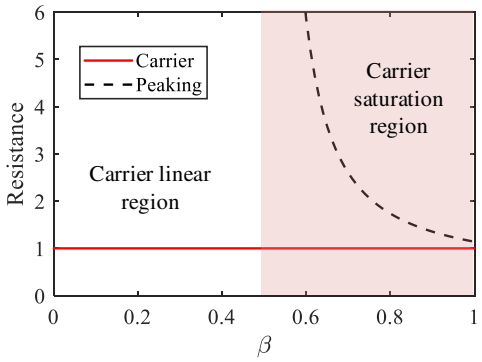

Fig. 7. Carrier and peaking resistance when $\beta_{bo} = 0.5$, $\alpha = 1.8$, $I_{max,c} = 0.5$ and $I_{max,p} = 1$.

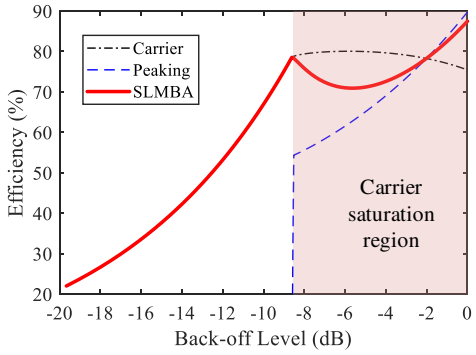

Fig. 8. Ideal efficiency performance of the proposed SLMBA and each branch along with back-off level.

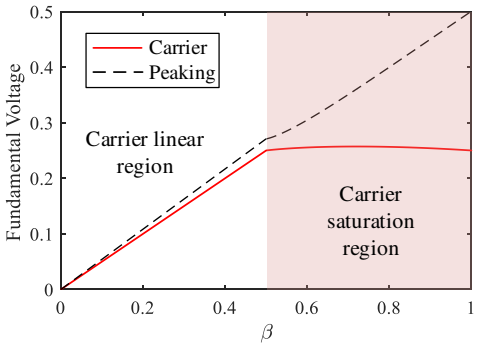

Fig. 9. Fundamental components of carrier and peaking voltage when $\beta_{bo} = 0.5$, $\alpha = 1.5$, $I_{max,c} = 0.5$ and $I_{max,p} = 1$.

is determined by the carrier and peaking PAs together. To ensure the optimal operation for the carrier and peaking CGs, Z_C should be set to $R_{opt,c}$, which is the optimal impedance required by the carrier CG. Thus, γ_c can be calculated by using Z_0 and $R_{opt,c}$. For the same reason, Z_P needs to achieve the optimal impedance required by the peaking CG $R_{opt,p}$ at the peak output power. Thus, γ_p can be calculated based on the following equation since we have already known γ_c,

$$R_{opt,p} = \frac{Z_0}{\gamma_p^2}(1 + \sqrt{2}\frac{i_{ca,max} \cdot \gamma_p}{i_{pk,max} \cdot \gamma_c}) \tag{21}$$

It should be noticed that, Z_C and Z_P are all pure resistances in the proposed configuration. Fig. 7 gives an example of the normalized carrier and peaking impedance along with β when $\beta_{bo} = 0.5$, $\alpha = 1.8$, $I_{max,c} = 0.5$ and $I_{max,p} = 1$, to show the proposed load modulation process.

Once Z_C and Z_P are determined, the performance of the proposed SLMBA can be described. In [14], it has been proven that the output power of LMBA equals the sum of all the output power generated by the employed CGs. Therefore, the fundamental output power of the proposed SLMBA can be calculated as,

$$P_o[1] = \frac{1}{2} i_{ca}[1]^2 \cdot Z_C + i_{pk}[1]^2 \cdot Z_P \tag{22}$$

The consumed DC power can be calculated as,

$$P_{dc} = i_{ca}[0] \cdot v_{dcc} + 2 i_{pk}[0] \cdot v_{dcp} \tag{23}$$

where v_{dcc} and v_{dcp} are the DC voltage of the carrier and peaking CGs, respectively.

Assume Z_C and Z_P achieve the optimal value for the related CGs when the amplitude of the related current achieves the maximum value, then they can be defined by the DC voltage and maximum current value as $Z_{C,opt} = 2v_{dcc}/I_{max,c}$ and $Z_{P,opt} = v_{dcp}/I_{pk,max}$. Therefore, we can calculate the efficiency of the proposed SLMBA by using $P_o[1]/P_{dc}$.

As mentioned earlier, the efficiency of the proposed SLMBA at the low power region is determined only by the carrier PA and the PA is driven to saturation when $\beta = \beta_{bo}$ based on the current relationship given in the previous subsection. If the optimal impedance for the class-B operation is set, the efficiency of the proposed SLMBA will achieve 78.5% when $\beta = \beta_{bo}$. At the high power region, because Z_C maintains the same value, the carrier PA will remain in high efficiency status if i_{ca} is not significantly reduced. The behavior of i_{ca} at high power region is constrained by the parameter α. On the other hand, when the peaking PA is turned on, the overall efficiency is pulled down. But as i_{pk} increases, the efficiency will gradually increase. This makes the efficiency characteristic of the SLMBA similar to that of the Doherty PA. Fig. 8 shows the ideal efficiency performance of the proposed SLMBA along with the back-off level when $\beta_{bo} = 0.5$, $\alpha = 1.5$, $I_{max,c} = 0.5$ and $I_{max,p} = 1$, as an example. In this situation, because the peaking balanced PAs generate more power than the carrier one, larger than 8 dB high-efficiency range is achieved with similar efficiency performance compared with Doherty PAs. The efficiency of each branch is also given in Fig. 8. It should be noticed that the efficiency at the peak power is higher than 78.5%, because the class-C mode peaking current model is employed in our analysis. The fundamental component of the carrier and peaking voltages in this situation are shown in Fig. 9.

It is relatively easy to achieve different OBO levels for the proposed SLMBA by changing the design parameters. Without changing the carrier impedance, different values of β_{bo} can be set by changing the carrier drain voltages to obtain different OBO power levels. In this situation, if we keep the peaking drain voltage unchanged to provide the same level peak output power, the value of $R_{opt,p}$ should be re-calculated because

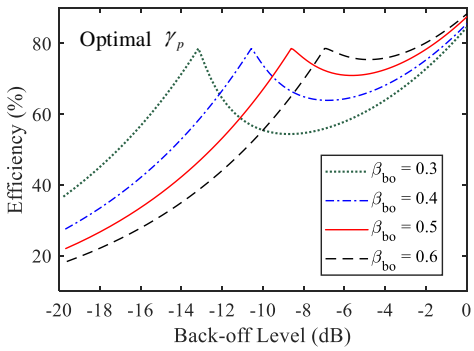

Fig. 10. Ideal efficiency performance of the proposed SLMBA versus back-off level with different parameters.

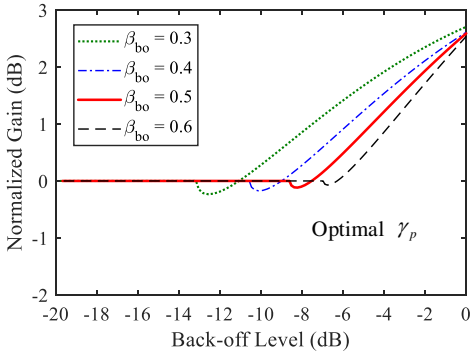

Fig. 11. Ideal gain performance of the proposed SLMBA versus back-off level with different parameters.

the conduction angle of the peaking class-C CG is different. Correspondingly, γ_p should also be re-calculated based on (21). Fig. 10 shows the efficiency performance of the proposed SLMBA with different β_{bo}. With the range from 0.6 to 0.3 of β_{bo}, the high efficiency range of the proposed SLMBA changes from 7 dB to 13.1 dB. The gain performance with different β_{bo} is shown in Fig. 11. It can be seen that, the gain shows a tendency to compress first and then expand due to "soft" turn on of the peaking PA.

Moreover, if we can consider a situation where we only change the value of β_{bo} while keep the value of $R_{opt,p}$ and γ_p unchanged, this means that we do not change the circuit parameters but only change the carrier drain voltage and the peaking gate bias. Fig. 12 presents the efficiency performance with different β_{bo} while keeping γ_p to the value designed for $\beta_{bo} = 0.5$. From Fig. 12 we can see that the efficiency at the peak power decreases compared with the results shown in Fig. 10. This is because the peaking impedance is not the optimal value. Nevertheless, the high efficiency range is not much reduced. The above analysis indicates that the high efficiency range of the proposed SLMBA can be re-configurable by only changing the carrier drain and peaking gate bias voltages without changing the designed circuits.

C. System Architecture of the Proposed SLMBA

In order to ensure that the output power of all the CGs can be combined successfully at saturation, it is important

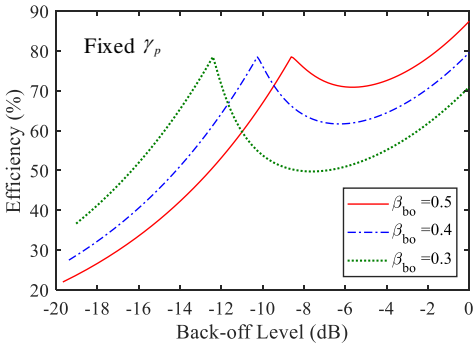

Fig. 12. Ideal efficiency performance of the proposed SLMBA versus back-off level with different β_{bo} and fixed γ_p.

to provide proper phase relationship at the different ports of the combining coupler for the proposed SLMBA. From the previous subsection, current relationship of $i_{p1} = i_{pk}$, $i_{p2} = -j \cdot i_{pk}$ and $i_c = j \cdot i_{ca}$ are used to build the system. This configuration actually gives the required phase relationship. To guarantee this configuration, several settings are required for the system block diagram shown in Fig. 1 where PA1 is the carrier amplifier while PA2 and PA3 form a peaking balanced PA pair. $i_{p1} = i_{pk}$ and $i_{p2} = -j \cdot i_{pk}$ are guaranteed by using the balanced amplifier mode, which means that an input coupler is required at the input of PA2 and PA3. Assume the phase at PA3 output is $0°$, and thus the phase at PA2 output will be $90°$. The required phase at PA1 output should now be $180°$ to satisfy $i_c = j \cdot i_{ca}$. Therefore, a transmission line is added to the input of PA1 to adjust the phase shift of the carrier branch. Moreover, a power divider is employed to divide the input power. It should be noticed that, based on the analysis from the previous subsection, ideally, a 1:2 power divider should be employed in the proposed SLMBA. However, in this situation, the gain will expand to some extent at the peak output power. To avoid this effect, a 1:1 power divider is thus recommended to be deployed. Due to the over-driven behavior of the carrier PA, changing the power division ratio will not affect the overall operation of the proposed SLMBA if we properly adjust the gate bias of the peaking PA, keeping the peaking PA turned-off at the back-off region.

III. Design of the Proposed RF-Input SLMBA

To design the proposed SLMBA, the operation parameters should be determined firstly. The configuration of $\beta_{bo} = 0.5$, $I_{max,c} = 0.5$ and $I_{max,p} = 1$ was used to provide larger than 8 dB OBO level. Commercial GaN HEMTs CGH40006s from Wolfspeed were used as the active devices for both the carrier and peaking PAs. Close to 65 Ω R_{opt} was suitable for the device when the drain supply voltage was set to 32 V based on the de-embedded load-pull simulation. To simplify the design and also achieve a larger OBO level, a lower drain supply voltage was used for the carrier device to limit the saturated current. The carrier drain voltage was set to 18 V considering 4 V knee voltage. Fig. 13 shows the simulated fundamental components of the carrier and peaking currents at this situation when the same value of the

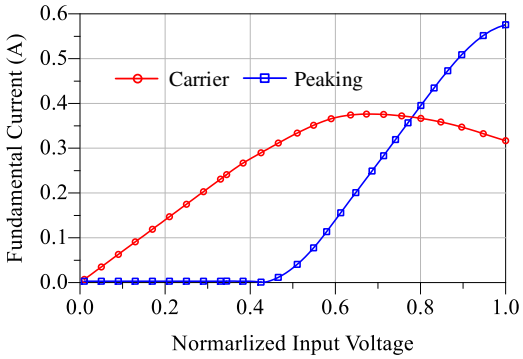

Fig. 13. Simulated fundamental components of the carrier and peaking currents.

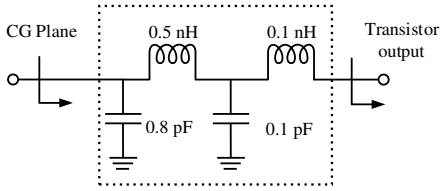

Fig. 14. Model of the parasitic and package parameters of the used transistors.

carrier R_{opt} was set. The current relationship is similar to the ideal fundamental current relationship as shown in Fig. 6. Because the fundamental component of the carrier current at the maximum output power level was almost equal to the value at back-off, $\alpha = 1.5$ was used here.

To avoid using a post-matching network and make the proposed SLMBA more compact, the port impedance of the output coupler was set to 50 Ω. Let's set Z_C equals to R_{opt}, then γ_c can be calculated from (19) as 0.877. Furthermore, γ_p can be calculated from (20) as 1.29. Therefore, the OMN realizing the matching from 65 Ω to 50 Ω should be designed for PA1, and OMNs realizing the matching from 65 Ω to 108 Ω should be designed for PA2 and PA3. All the above mentioned matching was from the CG planes to the coupler ports.

To design the OMNs, the model of the parasitic and package parameters of the used transistors was first built as shown in Fig. 14 based on the S-parameters of the transistor when it is turned off [31]. The OMNs employed the T-shaped transmission line (TL) structure with wideband characteristics in the band of 3.1-3.6 GHz. Due to the constant load feature of the carrier branch in the proposed SLMBA, the design of these OMNs was relatively easy. After designing the OMNs, stepped TLs were used to design the input matching networks (IMNs). A 500 Ω resistor was added at the gate bias path to provide high impedance condition while keeping the proper gate bias voltage at the same time. Two TL-based directional couplers and a Wilkinson power divider were then designed to ensure the power division and combining for the SLMBA. Moreover, a 50 Ω TL was added in front of the carrier IMN, adjusting the phase shift between the carrier and peaking branches to satisfy the relationship described in Fig. 1.

All the above mentioned circuits were designed on the 31 mil ROGERS 5880 substrate with dielectric constant of 2.2.

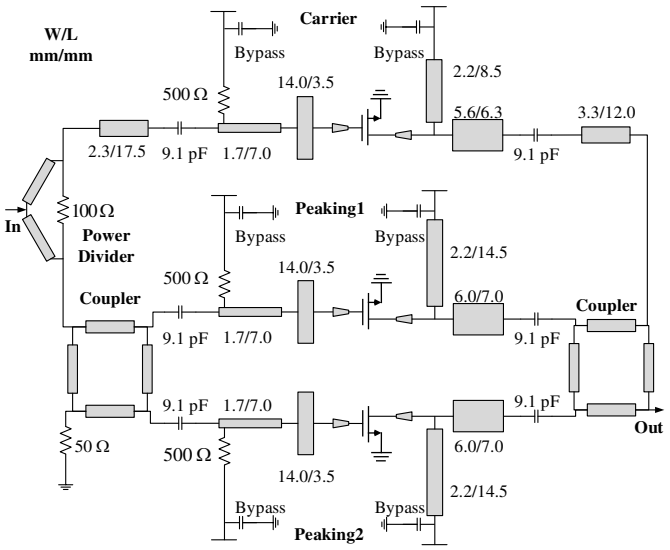

Fig. 15. Circuits detail of the proposed SLMBA.

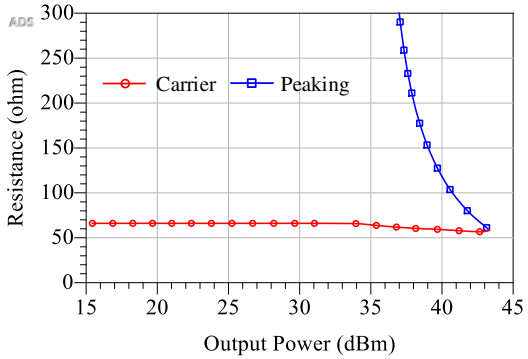

Fig. 16. Simulated matching resistance of the carrier and peaking devices versus output power at the CG planes at 3.35 GHz.

The entire circuits were EM-simulated using ADS Momentum and the specific sizes of the used TLs were optimized within a certain range to obtain better performance. Fig. 15 shows the circuits detail of the proposed SLMBA.

Fig. 16 presents the simulated matching resistance of the carrier and peaking devices versus output power at the CG planes at 3.35 GHz. We can see that, the carrier impedance is almost constant when the output power changes. This is the most important feature of the proposed SLMBA. Besides, at saturation, the matching resistance of the carrier and peaking devices become very close to the required R_{opt} at the same time. The simulated load modulation process shown in Fig. 16 is almost the same as the ideal one shown in Fig. 7. The load modulation process shown in fig. 16 indicates that the proposed SLMBA is successfully designed.

The simulated performance of the proposed SLMBA at different frequencies when the carrier drain supply voltage equals 18 V is shown in Fig. 17. Peak efficiency of 66.1-74.7% is achieved by the designed SLMBA with saturated power of 42.9 to 43.7 dBm. Back-off efficiency of 54.7-62.4%, 51.4-60.2% and 48.2-55.8% is obtained at 6, 8, 10 dB OBO region, respectively. It can be seen that, the proposed SLMBA

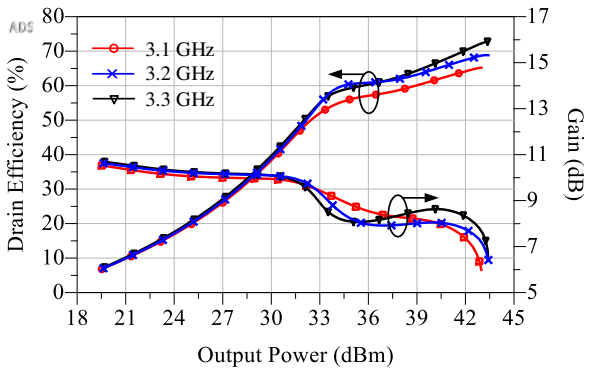

(a)

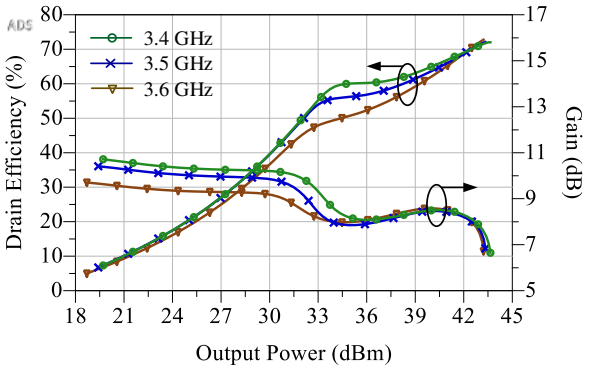

(b)

Fig. 17. Simulated drain efficiency and gain of the proposed DPA versus output power at (a) 3.1-3.3 GHz, (b) 3.4-3.6 GHz.

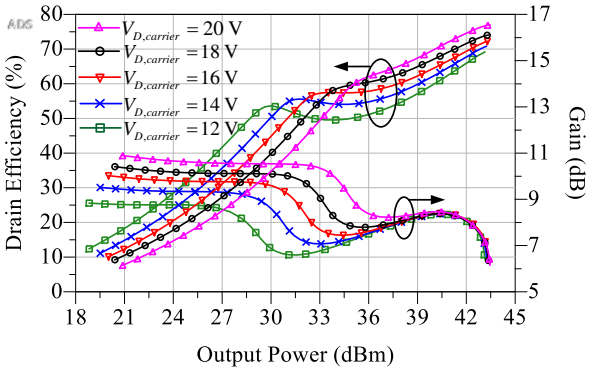

Fig. 18. Simulated drain efficiency and gain versus output power with different drain supply voltage at 3.35 GHz.

achieves excellent efficiency performance at deep OBO region within 500 MHz bandwidth. Fig. 18 presents the simulated drain efficiency and gain versus output power with different drain supply voltages at 3.35 GHz. In this simulation, the drain supply voltage of the carrier PA changes from 20 V to 12 V with 2 V step. Simultaneously, the gate bias of the peaking PAs change from -5.3 V to -4.7 V with 0.15 V step. The drain supply voltages of the peaking PAs and the gate bias of the carrier PA keep the same values. From Fig. 18 we can see that the high efficiency range is further extended. To better present the wideband performance of the proposed

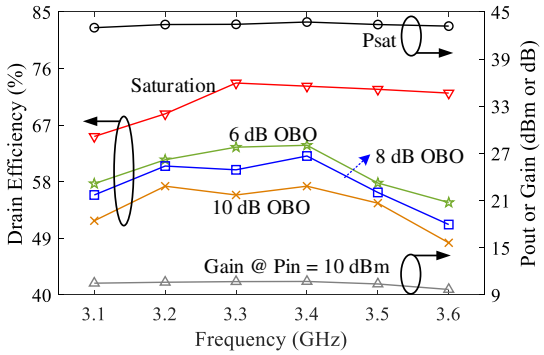

Fig. 19. Simulated performance at different operation frequencies.

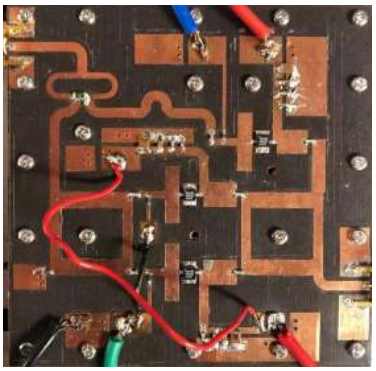

Fig. 20. Photograph of the fabricated SLMBA.

SLMBA, the simulated performance at different frequencies, when the drain supply voltage is set to 18 V, is shown in Fig. 19. It is worth mentioning that, the bandwidth of the SLMBA shown in this paper is not too wide because a narrow coupler was used in the design that limited the bandwidth. In principle, the proposed SLMBA has the potential to achieve wider bandwidth if wideband couplers are used.

IV. Experimental Results

The photograph of the fabricated SLMBA is shown in Fig. 20. The size of the entire circuit is 8.8 cm×8.9 cm. This size can be greatly reduced by using integrated couplers. The fabricated SLMBA was measured using both continuous-wave (CW) and wideband modulated signals. The drain supply voltage of 32 V for the peaking amplifier pair and quiescent current of 80 mA for the carrier PA were set during all the measurements. Different bias settings for the carrier drain and peaking gate supply voltages were employed to show the performance at deep OBO region. The CW and modulated signals were both generated by a vector signal generator, and the output power was measured using a spectrum analyzer. A broadband linear driver amplifier was employed to drive the SLMBA with enough input power.

A. Measurements under CW Signal Stimulation

The implemented SLMBA was firstly measured using CW signal at the centre frequency of 3.3 GHz using five different drain supply voltages of 20 V, 18 V, 16 V, 14 V and 12 V

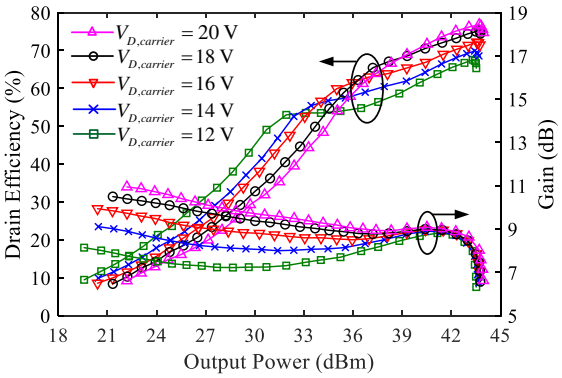

Fig. 21. Measured drain efficiency and gain versus the output power at different carrier drain bias voltages at 3.3 GHz.

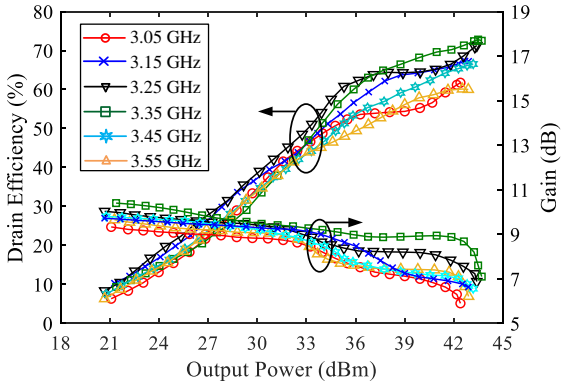

Fig. 22. Measured drain efficiency and gain versus the output power at different operation frequencies when the carrier drain bias voltage is set to 18 V.

for the carrier PA. Meanwhile, the peaking gate bias voltages of -5.55, -5.4 V, -5.15, -5 V, and -4.85 V were set in the four conditions, respectively. Fig. 21 shows the measured drain efficiency and gain versus the output power. When the drain supply voltage was set to 18 V, the proposed SLMBA achieves a maximum drain efficiency 74.8% with output power of 43.7 dBm. 64.9%/58.8%/50.1% back-off efficiency is obtained at 6/8/10 dB OBO, respectively. The SLMBA also presents 10.3 dB gain in the small signal region while compressing to 7.5 dB at saturation. When using 12 V drain supply voltage, the high efficiency range is obviously extended as shown in Fig. 21. Efficiency of 49.1% is achieved at 12.8 dB OBO. Meanwhile, the OBO range with higher than 52% efficiency is larger than 11.5 dB. It is important to notice that, the maximum output power maintains at 43.5 dBm, because the output power is mainly generated by the peaking PA pair.

To show the wideband performance, the proposed SLMBA was then measured from 3.05 GHz to 3.55 GHz with 50 MHz step. The designed frequency band with high back-off efficiency has slightly shifted due to fabrication variations and model inaccuracy of the active devices. In this measurement, the drain supply voltage of the carrier PA was set to 18 V. Fig. 22 presents the measured drain efficiency and gain versus the output power at different operation frequencies. To better present the wideband performance, the measured performance

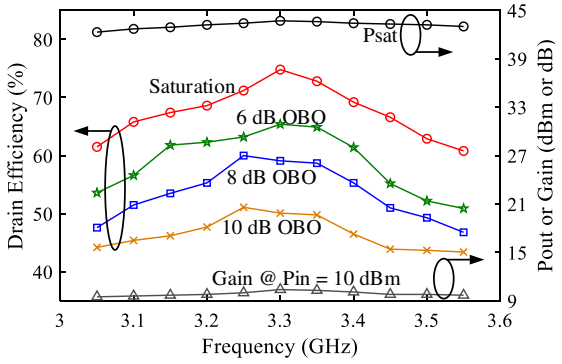

Fig. 23. Measured performance at different operation frequencies.

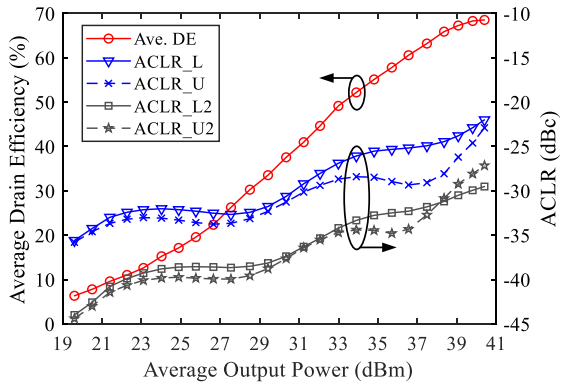

Fig. 24. Measured average efficiency and ACLR versus output power under 40 MHz 8 dB PAPR OFDM signal stimulation at 3.3 GHz.

versus the operation frequency is also given as shown in Fig. 23. The proposed SLMBA achieves 60.8% to 74.8% peaking efficiency with 42.3 to 43.7 dBm maximum output power and 9.5 to 10.3 dB small signal gain throughout the band. Back-of efficiency of 50.9-64.9%, 46.8-60.7% and 43.2-51.4 % are obtained at 6, 8 and 10 dB OBO region, respectively.

B. Measurements under Modulated Signal Stimulation

To evaluate the performance of the proposed SLMBA in actual wireless communication systems, three LTE-OFDM signals were employed to perform the measurement: 40 MHz 2-carrier with 8 dB PAPR, 80 MHz 4-carrier with 10 dB PAPR, and 200 MHz 10-carrier with 10 dB PAPR. The drain supply voltage of the carrier PA was set to 18 V in this measurement.

Fig. 24 shows measured average efficiency and ACLR without linearization versus average output power under 40 MHz 8 dB PAPR OFDM signal stimulation at 3.3 GHz. The proposed SLMBA presents excellent average efficiency performance and also good linearity. The measured average output power changes from 19.6 to 40.4 dBm while the ACLR maintains better than -21 dBc within the output power range. The proposed SLMBA achieves ACLR of better than -25 dBc with average efficiency of 63.2%. Besides, the average efficiency keeps higher than 49% at 33 dBm with ACLR better than -27.6 dBc.

Digital predistortion (DPD) was then performed to correct the nonlinearity of SLMBA. Because the linearization per-

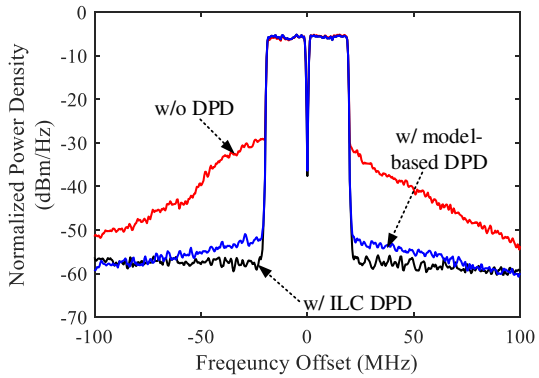

Fig. 25. Output spectrum under 40 MHz 8 dB PAPR OFDM signal stimulation with 35.5 dBm at 3.3 GHz.

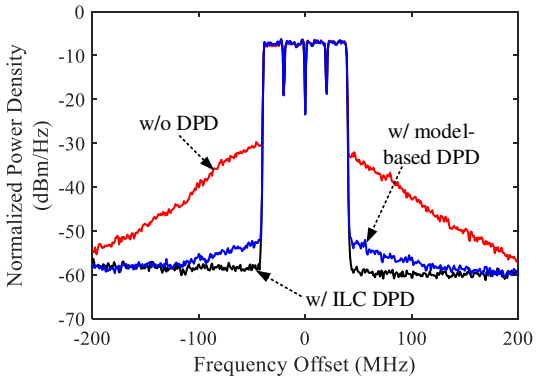

Fig. 26. Output spectrum under 80 MHz 10 dB PAPR OFDM signal stimulation with 33.8 dBm at 3.3 GHz.

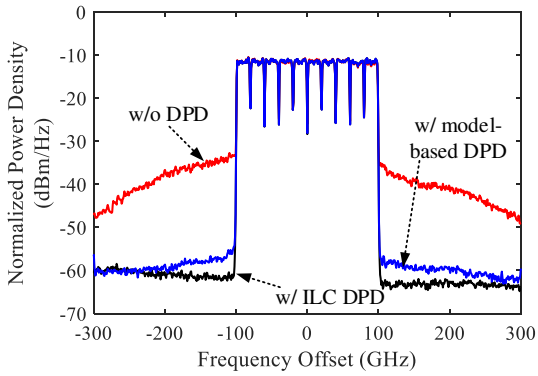

Fig. 27. Output spectrum under 200 MHz 10 dB PAPR OFDM signal stimulation with 33 dBm at 3.3 GHz.

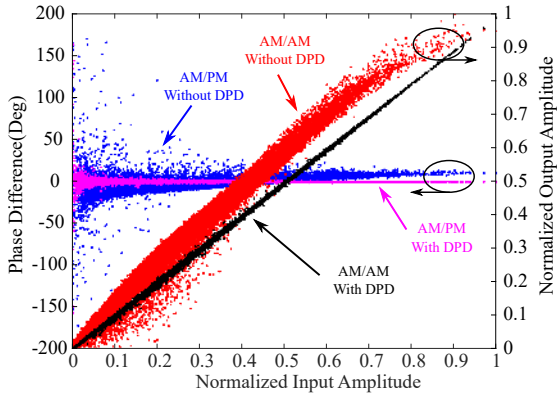

Fig. 28. AM/AM and AM/PM under 200 MHz 10 dB PAPR OFDM signal stimulation at 3.3 GHz.

formance heavily relies on which model we use in DPD, to remove the bias caused by the DPD model, we first employed the iterative learning control (ILC) algorithm [32] in the test. The ILC uses repeated sequences to iteratively generate a nearly ideal predistorted excitation which can linearize the PA to the best achievable linearity. In other words, the ILC test can reveal the linearity limit the PA can be best linearized to. After the ILC test, we measured the linearity performance using the Magnitude-Selective Affine (MSA) function model [33], called model-based DPD, to linearize the PA with a closed-loop estimator. The model-based DPD is implementable in a real system since it does not require repeated sequences but its performance can be worse than that of ILC. Fig. 25 shows the output spectrum without DPD, with ILC DPD and with model-based DPD. The ACLR is improved from -24.9 dBc to -51.8 dBc after ILC DPD performed and improved to -46.7 dBc with model-based DPD. The average efficiency is 57.8% with average output power of 35.5 dBm after model-based DPD performed.

To further test the performance under wideband signal stimulations, measurements under 4/10-carrier 80/200 MHz OFDM signals with 10 dB PAPR were then performed. Fig. 26 and Fig. 27 shows the output spectrum with and without DPD. For the 80 MHz signal, the ACPR is improved from -23.1 dBc to -50.7 dBc after ILC DPD performed and improved to -45.2 dBc with model-based DPD. The average efficiency is 49.9% with average output power of 33.8 dBm after model-based DPD. For the 200 MHz signal, the ACPR is improved from -21.1 dBc to -49.1 dBc after ILC DPD performed and improved to -43.9 dBc with model based DPD. The average efficiency is 48.2% with average output power of 33 dBm after model-based DPD. The AM/AM and AM/PM characteristics with and without model-based DPD for the 200 MHz signal are also given in Fig. 28. It can be seen the nonlinearity can be corrected very well after the model-based DPD performed.

C. Performance Comparison

Table. I summarizes the performance comparison of some recently reported high-efficiency PAs. Compared with other published high efficiency PAs, the proposed SLMBA shows excellent efficiency performance at both saturation and different OBO levels. Particularly, when driven by modulated signals with 200 MHz instantaneous bandwidth with 10 dB PAPR, 48.2% average efficiency was achieved by the proposed SLMBA while maintaining good linearity performance.

V. Conclusion

The theory and design methodology of an RF-input SLMBA is presented in this paper. The proposed SLMBA demonstrates the ability to achieve high efficiency, wide bandwidth and large high efficiency OBO ranges at the same time in both theory

TABLE I
PERFORMANCE COMPARISON OF RECENTLY PUBLISHED HIGH EFFICIENCY PAS.

Ref. (Year)	Arch. N/A	Freq (GHz)	Gain (dB)	η@Sat. (%)	OBO (dB)	η@OBO (%)	Pmax (dBm)	Signal BW (MHz)	PAPR (dB)	Pave (dBm)	η_{ave} (%)	ACLR (dBc)
[1]2016	Doherty	1.65-2.75	9.3-11.7	66-77	6	52-66	44.5-46.3	20	7.5	38	62	-48*
[3]2018	Doherty	3.3-3.75	11.8-13.5	58-71	8	44-55	48-48.8	40	8	40.7	53	-30#
[5]2019	3-stage Doherty	1.6-2.6	8.5-11	53-66	9.5	50-53	45.5-46	40	8.5	36.3	50	-50*
[11]2018	Doherty	4.7-5.3	9.2-10	52-57	9	29.7-33.1	39-39.5	40/ 160	7.4/ 7.4	32/ 32	42/ 42	-51.3*/ -44.3*
[16]2018	LMBA	1.7-2.5	9.9-13.2	48-58**	6	43-53**	48-48.9	20	9	39	40**	-49*
[17]2018	RF-input LMBA	2.4	12	67	6	54	45.6	10	7.5	38	47	-27#
[22]2015	SPA-D	2.0-2.7	8-14	58-70	6/ 9	36-65/ 45-66	40-42	10/ 20	7.8/ 8.2	31.4/ 30.8	50**/ 48**	-49.2*/ -39.2*
[26]2018	DEPA	1.8-3.8	7.6-10.8	42-62	8	41-51	44.3-46.5	400	8	37.5	45.6	-49.9*
[34]2016	Out -phasing	2.14	N/A	72	7	60	50.2	5	9.15	41	54.5	-34.2*
[35]2018	ET +Doherty	3.5	13	55**	6	49**	42	60/ 60	6/ 10	35.7/ 32.3	43.2**/ 38.7**	-42.3*/ -47*
[36]2016	Doherty	1.6-2.2	15-17	60-71	10	51-55	46-47	20	9.1	36	50	-48*
[37]2019	Out -phasing	1.9	13	70**	8	73**	44	3.84/ 10	9.5/ 9.5	34.5/ 34.5	59.5**/ 59.4**	-50.9*/ -45.3*
This Work	RF-input SLMBA	3.05-3.55	9.5-10.3	60.8-74.8	6/ 8/ 10	50.9-64.9/ 46.8-60.7/ 43.2-51.4	42.3-43.7	40/ 80/ 200	8/ 10/ 10	35.5/ 33.8/ 33	57.8/ 49.9/ 48.2	-46.7*/ -45.2*/ -43.9*
				50.6-62.5**	6/ 8/ 10	44.1-54.2**/ 40.9-55.1**/ 38.0-46.7**		40/ 80/ 200	8/ 10/ 10	35.5/ 33.8/ 33	50.9**/ 44.8**/ 43.6**	-46.7*/ -45.2*/ -43.9*

** - Power added efficiency, * - ACLR with DPD, # - ACLR without DPD

and realization. Excellent efficiency performance is achieved by the fabricated SLMBA at a very large OBO region for both CW and modulated signal measurements. The proposed architecture provides a new solution to improve the back-off efficiency at larger OBO levels while maintaining wideband performance. From the simulation and measurements results we can see that, despite the use of the over-driven carrier PA, the linearity of the proposed SLMBA is comparable with that of the PAs using other architectures. The reliability of SLMBA may need further verification due to the use of the large over-driven device. Nevertheless, to avoid extreme over-driven state, limiter or clipper can be introduced in the carrier branch to improve the reliability.

ACKNOWLEDGMENT

The authors would like to thank D. Lehane for helping us with the fabrication.

REFERENCES

[1] X. Chen, W. Chen, F. M. Ghannouchi, Z. Feng, and Y. Liu, "A broadband Doherty power amplifier based on continuous-mode technology," *IEEE Trans. Microw. Theory Techn.*, vol. 64, no. 12, pp. 4505–4517, Dec. 2016.

[2] W. Shi, S. He, X. Zhu, B. Song, Z. Zhu, G. Naah, and M. Zhang, "Broadband continuous-mode Doherty power amplifiers with noninfinity peaking impedance," *IEEE Trans. Microw. Theory Techn.*, vol. 66, no. 2, pp. 1034–1046, Feb. 2018.

[3] C. Huang, S. He, and F. You, "Design of broadband modified class-J Doherty power amplifier with specific second harmonic terminations," *IEEE Access*, vol. 6, pp. 2531–2540, 2018.

[4] J. Xia, M. Yang, Y. Guo, and A. Zhu, "A broadband high-efficiency Doherty power amplifier with integrated compensating reactance," *IEEE Trans. Microw. Theory Techn.*, vol. 64, no. 7, pp. 2014–2024, Jul. 2016.

[5] J. Xia, W. Chen, F. Meng, C. Yu, and X. Zhu, "Improved three-stage Doherty amplifier design with impedance compensation in load combiner for broadband applications," *IEEE Trans. Microw. Theory Tech.*, vol. 67, no. 2, pp. 778–786, Feb. 2019.

[6] Z. Yang, Y. Yao, M. Li, Y. Jin, T. Li, Z. Dai, F. Tang, and Z. Li, "Bandwidth extension of Doherty power amplifier using complex combining load with noninfinity peaking impedance," *IEEE Trans. Microw. Theory Tech.*, vol. 67, no. 2, pp. 765–777, Feb. 2019.

[7] J. Pang, S. He, C. Huang, Z. Dai, J. Peng, and F. You, "A post-matching Doherty power amplifier employing low-order impedance inverters for broadband applications," *IEEE Trans. Microw. Theory Techn.*, vol. 63, no. 12, pp. 4061–4071, Dec. 2015.

[8] X. Y. Zhou, S. Y. Zheng, W. S. Chan, X. Fang, and D. Ho, "Postmatching Doherty power amplifier with extended back-off range based on self-generated harmonic injection," *IEEE Trans. Microw. Theory Techn.*, vol. 66, no. 4, pp. 1951–1963, Apr. 2018.

[9] X. Y. Zhou, W. S. Chan, S. Y. Zheng, W. Feng, H. Liu, K. M. Cheng, and D. Ho, "A mixed topology for broadband high-efficiency Doherty power amplifier," *IEEE Trans. Microw. Theory Techn.*, vol. 67, no. 3, pp. 1050–1064, Mar. 2019.

[10] D. Gustafsson, C. M. Andersson, and C. Fager, "A modified Doherty power amplifier with extended bandwidth and reconfigurable efficiency," *IEEE Trans. Microw. Theory Techn.*, vol. 61, no. 1, pp. 533–542, Jan. 2013.

[11] X. Fang, A. Chung, and S. Boumaiza, "Linearity-enhanced Doherty power amplifier using output combining network with predefined AM-PM characteristics," *IEEE Trans. Microw. Theory Techn.*, pp. 1–10, 2018.

[12] X. Fang, H. Liu, K. M. Cheng, and S. Boumaiza, "Modified Doherty Amplifier With Extended Bandwidth and Back-Off Power Range Using Optimized Peak Combining Current Ratio," *IEEE Trans. Microw. Theory Techn.*, vol. 66, no. 12, pp. 5347–5357, Dec. 2018.

[13] L. Gupta, R. Jain, and G. Vaszkun, "Survey of Important Issues in UAV communication networks," *IEEE Commun. Surv. Tutor.*, vol. 18, no. 2, pp. 1123–1152, Secondquarter 2016.

[14] D. J. Shepphard, J. Powell, and S. C. Cripps, "An efficient broadband reconfigurable power amplifier using active load modulation," *IEEE Microw. Wirel. Compon. Lett.*, vol. 26, no. 6, pp. 443–445, Jul. 2016.

[15] P. H. Pednekar, E. Berry, and T. W. Barton, "RF-input load modulated balanced amplifier with octave bandwidth," *IEEE Trans. Microw. Theory Techn.*, vol. 65, no. 12, pp. 5181–5191, Dec. 2017.

[16] R. Quaglia and S. Cripps, "A load modulated balanced amplifier for telecom applications," *IEEE Trans. Microw. Theory Techn.*, vol. 66, no. 3, pp. 1328–1338, Mar. 2018.

[17] P. H. Pednekar, W. Hallberg, C. Fager, and T. W. Barton, "Analysis and design of a Doherty-like RF-input load modulated balanced amplifier," *IEEE Trans. Microw. Theory Techn.*, vol. 66, no. 12, pp. 5322–5335, Dec. 2018.

[18] T. Cappello, P. H. Pednekar, C. Florian, Z. Popovic, and T. W. Barton, "Supply modulation of a broadband load modulated balanced amplifier," in *2018 IEEE MTT-S International Microwave Symposium (IMS)*, Jun. 2018, pp. 304–307.

[19] J. R. Powell, D. J. Shepphard, R. Quaglia, and S. C. Cripps, "A power reconfigurable high-efficiency X -band power amplifier mmic using the load modulated balanced amplifier technique," *IEEE Microw. Wirel. Compon. Lett.*, vol. 28, no. 6, pp. 527–529, Jun. 2018.

[20] D. Seebacher, W. Bösch, P. Singerl, and C. Schuberth, "The impact of the Q-factor of the parasitic capacitances of RF transistors on their load modulation capabilities," in *2014 10th Conference on Ph.D. Research in Microelectronics and Electronics (PRIME)*, Jun. 2014, pp. 1–4.

[21] B. Merrick, J. King, and T. Brazil, "A wideband sequential power amplifier," in *2014 IEEE MTT-S International Microwave Symposium(IMS)*, Jul. 2014, pp. 1–3.

[22] X. A. Nghiem, J. Guan, and R. Negra, "Broadband sequential power amplifier with Doherty-type active load modulation," *IEEE Trans. Microw. Theory Techn.*, vol. 63, no. 9, pp. 2821–2832, Sep. 2015.

[23] T. Lehmann and R. Knoechel, "Sequential power amplifiers with adaptable combiners," in *2009 IEEE MTT-S International Microwave Symposium Digest*, Jul. 2009, pp. 425–428.

[24] Y. Cao, H. Lyu, and K. Chen, "Load modulated balanced amplifier with reconfigurable phase control for extended dynamic range," in *2019 IEEE MTT-S International Microwave Symposium (IMS)*, Jun. 2019, pp. 1335–1338.

[25] J. Pang, S. He, Z. Dai, C. Huang, J. Peng, and F. You, "Design of a post-matching asymmetric Doherty power amplifier for broadband applications," *IEEE Microw. Wirel. Compon. Lett.*, vol. 26, no. 1, pp. 52–54, Jan. 2016.

[26] P. Saad, R. Hou, R. Hellberg, and B. Berglund, "A 1.8-3.8 GHz power amplifier with 40% efficiency at 8-dB power back-off," *IEEE Trans. Microw. Theory Tech.*, vol. 66, no. 11, pp. 4870–4882, Nov. 2018.

[27] ——, "Ultra-wideband Doherty-like power amplifier," in *2018 IEEE MTT-S International Microwave Symposium(IMS)*, Jul. 2018, pp. 1215–1218.

[28] ——, "An 80W power amplifier with 50% efficiency at 8 dB power back-off over 2.6-3.8 GHz," in *2019 IEEE MTT-S International Microwave Symposium(IMS)*, Jul. 2019, pp. 1328–1330.

[29] W. Shi, S. He, F. You, H. Xie, G. Naah, Q. Liu, and Q. Li, "The influence of the output impedances of peaking power amplifier on broadband Doherty amplifiers," *IEEE Trans. Microw. Theory Techn.*, vol. 65, no. 8, pp. 3002–3013, Aug. 2017.

[30] J. Moon, S. Jee, J. Kim, J. Kim, and B. Kim, "Behaviors of Class-F and Class-F^{-1} amplifiers," *IEEE Trans. Microw. Theory Techn.*, vol. 60, no. 6, pp. 1937–1951, Jun. 2012.

[31] M. Li, J. Pang, Y. Li, and A. Zhu, "Ultra-wideband dual-mode Doherty power amplifier using reciprocal gate bias for 5G applications," *IEEE Trans. Microw. Theory Tech.*, vol. 67, no. 10, pp. 4246–4259, Oct. 2019.

[32] J. Chani-Cahuana, P. N. Landin, C. Fager, and T. Eriksson, "Iterative learning control for RF power amplifier linearization," *IEEE Trans. Microw. Theory Techn.*, vol. 64, no. 9, pp. 2778–2789, Sep. 2016.

[33] Y. Li, W. Cao, and A. Zhu, "Instantaneous sample indexed magnitude-selective affine function-based behavioral model for digital predistortion of RF power amplifiers," *IEEE Trans. Microw. Theory Techn.*, vol. 66, no. 11, pp. 5000 – 5010, Nov. 2018.

[34] T. W. Barton, A. S. Jurkov, P. H. Pednekar, and D. J. Perreault, "Multi-way lossless outphasing system based on an all-transmission-line combiner," *IEEE Trans. Microw. Theory Techn.*, vol. 64, no. 4, pp. 1313–1326, Apr. 2016.

[35] D. Fishler, T. Cappello, W. Hallberg, T. W. Barton, and Z. Popovic, "Supply modulation of a linear doherty power amplifier," in *48th European Microwave Conference (EuMC)*, Sep. 2018, pp. 519–522.

[36] J. Xia, M. Yang, and A. Zhu, "Improved Doherty amplifier design with minimum phase delay in output matching network for wideband application," *IEEE Microw. Wirel. Compon. Lett.*, vol. 26, no. 11, pp. 915–917, Nov. 2016.

[37] H. Chang, Y. Hahn, P. Roblin, and T. W. Barton, "New mixed-mode design methodology for high-efficiency outphasing chireix amplifiers," *IEEE Trans. Circuits Syst. Regul. Pap.*, vol. 66, no. 4, pp. 1594–1607, Apr. 2019.

Jingzhou Pang (S'13-M'16) received the B.S. degree in electrical engineering and Ph. D. degree in circuits and systems from University of Electronic Science and Technology of China (UESTC), Chengdu, China, in 2010 and 2016, respectively. In December 2016, he joined Huawei Technologies Company Ltd., where he was a senior engineer in charge of the research and development of 5G high efficiency power amplifiers and transmitters. He is currently with the RF and Microwave Research Group at University College Dublin (UCD) as a research fellow. His research interests include broadband high-efficiency power amplifier systems, bandwidth extension techniques for high-efficiency transmitters and MMIC power amplifier design for RF/microwave and millimeter-wave applications.

Jingzhou Pang was a recipient of the EDGE Marie Sklodowska-Curie Individual Fellowship. He was a recipient of third Place Award of the High Efficiency Power Amplifier Student Design Competition, IEEE Microwave Theory and Techniques Society (IEEE MTT-S) International Microwave Symposium (IMS) in 2013.

Yue Li (S'17) received the B.E. degree in information engineering from Southeast University, Nanjing, China, in 2016. He is currently working towards the Ph.D. degree at University College Dublin, Dublin, Ireland.

He is currently with the RF and Microwave Research Group, UCD. His current research interests include behavioral modeling and digital predistortion for RF power amplifiers.

Meng Li (S'14) received the B.S. degree in Electromagnetic Field and Radio Technology and M.S. degree in Electromagnetic Field and Microwave Technology from University of Electronic Science and Technology of China (UESTC), Chengdu, China, in 2012 and 2015, respectively, and is currently working towards the Ph.D degree at University College Dublin (UCD), Dublin, Ireland.

She is currently with the RF and Microwave Research Group, UCD. Her research interests mainly focus on broadband high-efficiency power amplifiers and MMIC power amplifier design for RF/microwave and millimeter-wave applications.

Yikang Zhang received the B.E. degree in electronic science and technology from China University of Mining and Technology, Xuzhou, China, in 2015. He is currently pursuing his Ph.D. degree in Electronic Engineering at University of Science and Technology of China, Hefei, China. From September 2018 to July 2019, he joined the IoE2 Laboratory, School of Electrical and Electronic and Engineering, University College Dublin, Dublin, Ireland, as a Visiting Ph.D. student. His research interests include digital predistortion linearization, nonlinear system identification algorithms and machine learning.

Xin Yu Zhou (S'15-M'16) was born in Tsingtao, Shandong Province, China. He received the M.Sc. and Ph.D. degrees in electronic engineering from City University of Hong Kong, Kowloon, Hong Kong, in 2014 and 2018, respectively.

From 2014 to 2015, he was a Research Assistant with the SYSU-CMU shunde international joint research institute. He is currently a Postdoctoral Fellow with the Department of Electronic Engineering at the City University of Hong Kong, Kowloon, Hong Kong. His current research interests include broadband, high efficient, high linear hybrid power amplifier for microwave applications and MMIC power amplifier design for millimeter-wave applications.

Dr. Zhou was a recipient of First Place Award of the High Efficiency Power Amplifier Student Design Competition, IEEE Microwave Theory and Techniques Society (IEEE MTT-S) International Microwave Symposium (IMS) in 2017 and a recipient of Second Place Award of the same Student Design Competition in 2018.

He is currently with the RF and Microwave Research Group, UCD. His current research interests include behavioral modeling and digital predistortion for RF power amplifiers.

Zhijiang Dai (M'19) received the B.S. and Ph.D. degrees in electrical engineering from the University of Electronic Science and Technology of China, Chengdu, China, in 2011 and 2017, respectively. From 2017 to 2018, he was a research engineer with Huawei Technologies, where he focused on the study of MIMO wireless communication systems.

He is currently a Lecturer with the School of Microelectronics and Communication Engineering, Chongqing University, Chongqing, China. His research interests lie in the area of automatic matching techniques of PA, wideband and linear RF PA design, MIMO system.

Anding Zhu (S'00-M'04-SM'12) received the Ph.D. degree in electronic engineering from University College Dublin (UCD), Dublin, Ireland, in 2004.

He is currently a Professor with the School of Electrical and Electronic Engineering, UCD. His research interests include high-frequency nonlinear system modeling and device characterization techniques, high-efficiency power amplifier design, wireless transmitter architectures, digital signal processing, and nonlinear system identification algorithms. He has published more than 130 peer-reviewed journal and conference articles.

Prof. Zhu is an elected member of MTT-S AdCom, the Chair of the Electronic Information Committee and the Vice Chair of the Publications Committee. He is also the Chair of the MTT-S Microwave High-Power Techniques Committee. He served as the Secretary of MTT-S AdCom in 2018. He was the General Chair of the 2018 IEEE MTT-S International Microwave Workshop Series on 5G Hardware and System Technologies (IMWS-5G) and a Guest Editor of the IEEE TRANSACTIONS ON MICROWAVE THEORY AND TECHNIQUES on 5G Hardware and System Technologies. He is currently an Associate Editor of the IEEE Microwave Magazine and a Track Editor of the IEEE TRANSACTIONS ON MICROWAVE THEORY AND TECHNIQUES.